Free Drainage in Aqueous Foams: Model and Experimental Study

S. A. Magrabi, B. Z. Dlugogorski, and G. J. Jameson
ARC Special Research Centre for Multiphase Processes and Dept. of Chemical Engineering, The University of Newcastle, Callaghan, NSW 2308 Australia

Free drainage in compressed-air foams were studied experimentally and theoretically. The time evolution of liquid holdup profiles in a 0.2-m-high by 0.29-m-diameter foam column was determined at various heights by measuring sonic velocity. A new experimental technique was devised to measure the true drainage rate of surfactant solution leaving the foam column. A drainage model was outlined to predict the discharge rate and evolution of the liquid-fraction profile in aqueous foams. The model led to the formulation of a nonlinear partial differential equation in which the liquid fraction was used explicitly as a dependent variable. The model was applied with one adjustable parameter to simulate drainage in foams made from fluorocarbon surfactants containing mobile plateau border and film walls. The liquid-fraction profiles, drainage rates, and final equilibrium liquid profiles depended strongly on the surface mobility of plateau border and film walls; the bubble size; and therefore on the coarsening history in the foam under study. Over longer time periods this model needs to be coupled with interbubble gas diffusion to account for coarsening-induced drainage.

Introduction

Soap froths, shaving foams, and fire-fighting foams are all common occurrences of aqueous foams in our daily lives. Aqueous foams are primarily evolving dispersions of gas bubbles in a relatively smaller volume of liquid. Foams evolve by three basic processes encompassing the gravitational drainage from the films and channels separating the foam bubbles; the coalescence of adjacent bubbles due to the rupture of interbubble lamellae, and Ostwald ripening, which is a coarsening process caused by interbubble gas transport. While coalescence and gravitational drainage can be limited by the use of suitable surfactants, coarsening is arduous to minimize and eventually contributes to foam collapse. However, slower drainage delays coarsening due to thicker lamellae and less steep pressure gradients between bubbles.

Coarsening is a difficult phenomenon to measure, hence the drainage rate, the time-dependent flow of liquid from a foam is often used to characterize the degree of water retention ability of a foam. Previous work by the authors on bubble growth in foams exhibited three growth regimes (Magrabi et al., 1999): the initial phase where the bubble growth is controlled by drainage; an intermediate phase exhibiting drainage and diffusion control; and the final phase where bubble growth is governed by diffusion. In this article, we focus on modeling the drainage and the evolution of liquid-fraction profiles in aqueous foams.

Free drainage due to gravity in an initially uniform column leads to a gradient in the liquid fraction, with the amount of liquid increasing from the top to the bottom of the foam. Typically, foams are comprised of polyhedral gas bubbles with liquid residing in the lamellae between the bubbles. The regions where three lamellae meet are called plateau borders and are channels for liquid flow (the terms plateau borders and channels will be used interchangeably in this article). The region between four touching bubbles where four plateau borders meet forms a vortex or node. Liquid drains from the lamellae to the plateau borders, which transfer liquid through the network of vertices and then finally out of the foam.

Over the last ten years, many models have been developed to simulate foam drainage (Goldfarb et al., 1988; Narsimhan, 1991; Fortes and Coughlan, 1994; Podual et al., 1996; Verbist et al., 1996; Bhakta and Ruckenstein, 1997), to list a few. The

Correspondence concerning this article should be addressed to B. Z. Dlugogorski. Present address of S. A. Magrabi: Holmes Fire and Safety, Sydney, Australia.

model developed by Verbist et al. (1996) in terms of the cross-sectional area of plateau borders, follows the drainage equation first derived by Goldfarb et al. (1988) and incorporates liquid flow through plateau borders, but ignores liquid flow in films. The approach used by Bhakta and Ruckenstein (1997) essentially follows that of Narsimhan (1991), and embodies both film and plateau border drainage together with coalescence, disjoining pressure effects, surfactant effects, and more detailed geometrical parameters to approximate the foam structure. Ramani et al. (1992) and Podual et al. (1996) modeled both film and plateau border foam drainage based on the pentagonal dodecahedral and β-tetrakaidecahedral bubble shapes, respectively, taking into account the surface mobility of plateau border and film walls. Fortes and Coughlan (1994) simulated foam drainage by associating plateau borders and vertices with vertically stacked pools that are connected by channels through which liquid drains. Recent contributions to modeling foam drainage have been made by Koehler et al. (1998, 1999), who have followed the Verbist et al. (1996) approach.

In this article, we reformulate the initial model of Bhakta and Ruckenstein (1995) to obtain a drainage equation similar to that developed by Verbist et al. (1996). In contrast to Verbist et al. (1996), however, the present equation uses liquid fraction rather than the cross-sectional area of plateau borders as a dependent variable. This allows for direct prediction of liquid-fraction holdup and convenient comparison with experiments, which normally involve measurements of liquid fraction.

A new method for measuring the true drainage rate from a foam column is outlined in this article. This is followed by the development of the drainage model leading to the drainage equation itself. Finally, comparisons between the modeled and experimental liquid-fraction profiles, and between the calculated and measured drainage rates, are presented.

Experiment

A compressed-air foam generator (Gardiner et al., 1998a; Magrabi et al., 1999) was used to produce a foam column (0.2 m high by 0.29 m diameter) of uniform liquid fraction in a Perspex cylinder, as shown in Figure 1. The foam solution (or surfactant solution) used in this study was prepared by diluting a 3% generic aqueous-film-forming fire-fighting foam concentrate with 97% deionized water. The composition of this foam concentrate is listed elsewhere (Gardiner et al., 1998a; Magrabi et al., 1999).

Liquid from the foam column was allowed to drain freely under the influence of gravity via a discharge outlet at the bottom of the Perspex cylinder. A new technique was devised to allow only the drained liquid to flow out of the foam column and prevent any foam from flowing out of the discharge outlet. Previously, a number of techniques were used to pre-

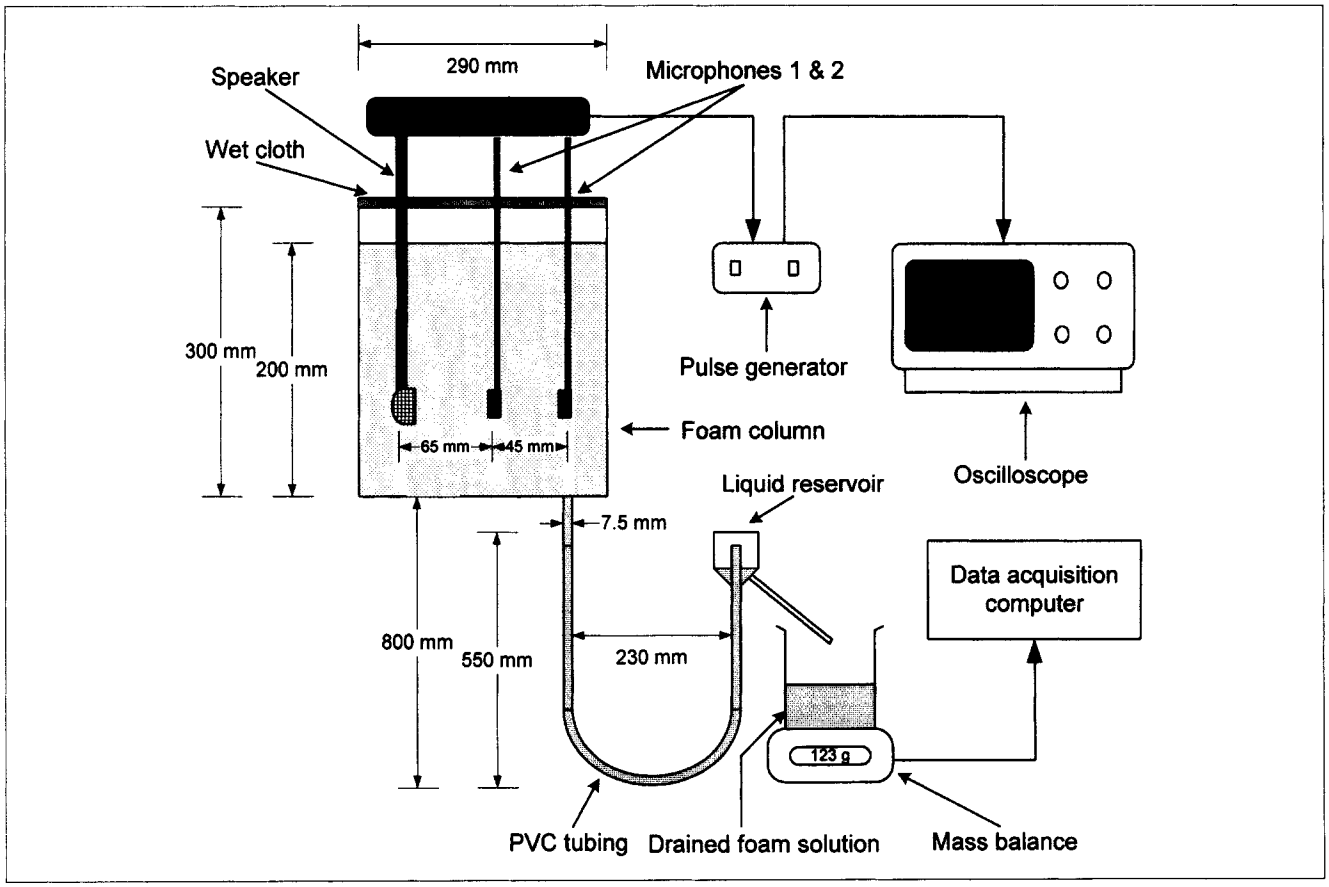

Figure 1. Experimental setup for foam drainage studies; not to scale.

vent foam from leaving the holding container and to allow only the foam solution to drain out. Essentially, these methods constituted the use of obstructions in the discharge outlet, including fine-grade steel wool (Magrabi et al., 2000); adjustable tap (Persson, 1992); filter paper, fine mesh, cloth, and dams (Isaksson and Persson, 1997). We observed that all these methods induce resistance to flow in the discharge outlet and dampen the drainage rate from the foam layer. The technique used in this article allows only foam solution to flow out from the holding container without any damping effect and gives the true drainage rate from the foam column.

The method encompasses the use of a manometer type U-tube setup made of PVC tubing, as shown in Figure 1. The U-tube is filled with foam solution of the same concentration as that used to generate the foam column. Being of lower density than the foam solution, the foam in the Perspex cylinder floats on top of the foam solution in the U-tube. Hence, at the outset of the trial, the liquid in the U-tube balances the foam mass in the column. As the liquid begins to drain from the foam column, it pushes the liquid out of the U-tube, giving the true drainage rate from the foam column. The free end of the U-tube leads to a liquid reservoir containing foam solution, which prevents the entrainment of air bubbles in the U-tube. The discharge outlet from the reservoir directs the flow to an electronic balance, which registers the drainage rate from the foam column with time.

The sonic velocity method (Gardiner et al., 1998b) was used to measure the liquid fraction φ as a function of height in the foam column. This approach involves the measurement of the velocity of sound in foam by immersing two microphones and a speaker into the foam sample, and using an oscilloscope to measure the time lag between the detection by the microphones of a square pulse (frequency $\approx$ 3400 Hz) produced by the speaker. The sonic velocity in a foam v_{sf} can be related to the liquid fraction φ by treating the foam to be a mixture composed of a compressible gas satisfying the ideal gas law and an incompressible liquid (Wood, 1941):

$$v_{sf} = \sqrt{\frac{\gamma P_a}{\rho}\left(\frac{1}{\varphi(1-\varphi)}\right)}, \tag{1}$$

where $\gamma = C_p/C_v$ for the isentropic expansion of an ideal gas. For the acoustic frequencies and bubble sizes used in the present measurements, there is no effect of bubble resonance on bubble breakup and coalescence (Manasseh, 1997).

Foam Drainage Equation

In the model development, we assume that all the liquid in the foam is present in the plateau borders and the amount of surfactant solution left in the lamellae is negligible. The flow of solution results in viscous dissipation, which in the model is considered to occur in plateau borders with no account taken for the dissipation in the vertices. Neglecting the inertia, the flow of viscous solution in the channels follows the Stokes equation:

$$\mu\nabla^2 u + \rho g - \frac{\partial p}{\partial z} = 0, \tag{2}$$

where the symbols have their standard meaning of viscosity (μ), velocity (u), density (ρ), gravitational constant (g), pressure (p), and z denotes vertical coordinates. By taking pressure within bubbles p_b as constant and considering the foam to consist of uniform-sized bubbles, the pressure in the channels follows from the Laplace and Young law as

$$p = p_b - \frac{\sigma}{r_c}, \tag{3}$$

where σ and r_c represent the surface tension and the radius of curvature of plateau borders, respectively. If N denotes the number of bubbles per unit volume, n_p is the number of plateau borders per bubble, a_p stands for the cross-sectional area of a plateau border, l signifies the length of a channel, V denotes the bubble volume, and φ ($Nn_p a_p l$) is the liquid fraction, it can be shown that (Narsimhan and Ruckenstein, 1986)

$$N = \frac{1-\varphi}{V}, \qquad a_p = \frac{V}{n_p l}\frac{\varphi}{1-\varphi}, \qquad r_c = \left(\frac{V}{\delta n_p l}\frac{\varphi}{1-\varphi}\right)^{1/2}, \tag{4}$$

where the extreme right expression follows from the relationship between the area of a plateau border channel and curvature of the channel wall: $a_p = (3^{1/2} - (\pi/2))r_c^2$, $\delta = 3^{1/2} - (\pi/2)$ (Goldshtein et al., 1996).

By combining Eqs. 3 and 4 and differentiating, one can obtain an expression for the pressure gradient in the channel:

$$\frac{\partial p}{\partial z} = \frac{\sigma}{2}\left(\frac{\delta n_p l}{V}\right)^{1/2}(1-\varphi)^{-1/2}\varphi^{-3/2}\frac{\partial \varphi}{\partial z}. \tag{5}$$

It can also be demonstrated that for a fully developed flow in a triangular channel with the effect of surface viscosity accounted for by the velocity coefficient c_v (Bhakta and Ruckenstein, 1997)

$$\mu\nabla^2 u = -\frac{20\sqrt{3}}{c_v}\frac{\mu v}{a_p} = -\frac{20\sqrt{3}}{c_v}\frac{n_p l}{V}\frac{1-\varphi}{\varphi}\mu v, \tag{6}$$

where v denotes the average velocity in a plateau border. Replacing Eqs. 5 and 6 in Eq. 2 leads to an expression for the average velocity in a plateau border in terms of the liquid fraction:

$$v = \frac{c_v}{20\sqrt{3}\,\mu}\frac{V}{n_p l}\frac{\varphi}{1-\varphi}\left[\rho g - \frac{\sigma}{2}\left(\frac{\delta n_p l}{V}\right)^{1/2}(1-\varphi)^{-1/2}\varphi^{-3/2}\frac{\partial \varphi}{\partial z}\right]. \tag{7}$$

By carrying out a mass balance over an infinitesimal horizontal element of the foam column, Bhakta and Ruckenstein (1995) showed that

$$\frac{\partial \varphi}{\partial t} + \frac{b}{e}\frac{\partial}{\partial z}(\varphi v) = 0, \tag{8}$$

where b (equals 3/15) is an average constant due to random orientation of plateau borders in the foam structure composed of pentagonal dodecahedra, and e (equals 0.816) is yet another constant related to the channel length and the radius of a sphere whose volume equals that of a foam cell r ($l = er$). Substituting Eq. 7 into Eq. 8 yields

$$\frac{\partial \varphi}{\partial t} + \frac{1}{f\mu}\frac{V}{n_p l}\frac{\partial}{\partial z}\left\{\left(\frac{\varphi^2}{1-\varphi}\right)\left[\rho g - \frac{\sigma}{2}\left(\frac{\delta n_p l}{V}\right)^{1/2}(1-\varphi)^{-1/2}\varphi^{-3/2}\frac{\partial \varphi}{\partial z}\right]\right\} = 0, \quad (9)$$

where a new constant f combines all other constants introduced so far:

$$f = \frac{20\sqrt{3}}{c_v}\frac{e}{b}. \quad (10)$$

We now define nondimensional variables τ and ζ, according to $t = t_o\tau$ and $z = z_o\zeta$, where

$$t_o = \frac{f\mu\sigma\delta^{1/2}(n_p l)^{3/2}}{2V^{3/2}(\rho g)^2}, \quad (11)$$

and

$$z_o = \frac{\sigma(\delta n_p l)^{1/2}}{2\rho g V^{1/2}}. \quad (12)$$

Our nondimensionalization is similar in nature to that used by Koehler et al. (1998) and avoids the problem of very small time steps if t_o is taken as equal to $\mu\delta^{1/4}(\sigma\rho g)^{-1/2}$, as done by Verbist et al. (1996). Using Eqs. 11 and 12, Eq. 9 assumes the following form:

$$\frac{\partial \varphi}{\partial \tau} + \frac{\partial}{\partial \zeta}\left[\frac{\varphi^2}{1-\varphi} - \frac{\varphi^{1/2}}{(1-\varphi)^{3/2}}\frac{\partial \varphi}{\partial \zeta}\right] = 0. \quad (13)$$

For a fresh foam generated with compressed air (Magrabi et al., 1999), the liquid fraction profile in the foam column is initially uniform, that is $\varphi = \varphi_o$ at $\tau = 0$ and for all ζ. Figure 2 illustrates the application of the drainage model to the foam column together with a summary of the dimensionless groups, initial, and boundary conditions. The top boundary condition reflects no flow of surfactant solution entering the foam column from above (at $\zeta = 0$), and is given as

$$\frac{\partial \varphi}{\partial \zeta} - \varphi^{3/2}(1-\varphi)^{1/2} = 0. \quad (14)$$

At the bottom of the foam column ($\zeta = \zeta_b$), the liquid fraction corresponds to that of randomly packed spheres, $\varphi_b = 0.26$ (Bhakta and Ruckenstein, 1997), after the onset of drainage. Prior to the commencement of drainage, a no-flow boundary condition is implemented.

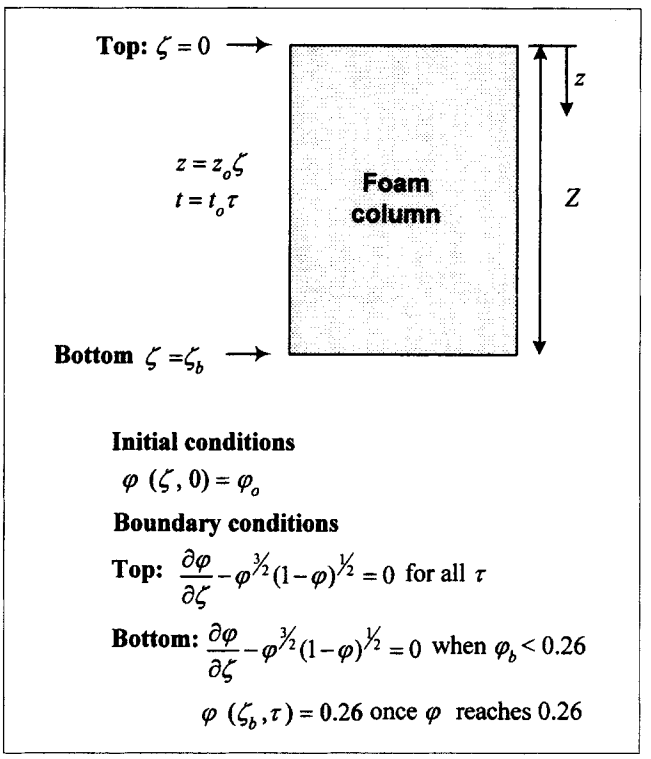

Figure 2. Application of the drainage model to the foam column.

The figure summarizes the dimensionless groups, the initial and boundary conditions applied in the modeling. In the calculations performed in this work, ζ_b was considered stationary.

The nondimensional expression for the flux of surfactant solution leaving the foam column is

$$q_b'' = \frac{\varphi_b^2}{1-\varphi_b} - \frac{\varphi_b^{1/2}}{(1-\varphi_b)^{3/2}}\left.\frac{\partial \varphi}{\partial \zeta}\right|_{\zeta=\zeta_b}, \quad (15)$$

which corresponds to the term in brackets in Eq. 13 evaluated at the boundary. As the foam drains and the surfactant solution accumulates below the foam layer, the bottom boundary moves up, ξ_b is a function of time and can be obtained from the following expression as shown in Appendix A:

$$\zeta_b(\tau) = \zeta_b(\tau = 0) - \frac{\varphi_b^2}{(1-\varphi_b)^2}\tau + \frac{\varphi_b^{1/2}}{(1-\varphi_b)^{5/2}}\int_o^\tau \left.\frac{\partial \varphi}{\partial \zeta}\right|_{\zeta=\zeta_b} d\tau'. \quad (16)$$

For relatively dry foams (e.g., $\varphi_o = 0.05$), such as those considered in this study, the interface between foam and surfactant solution can be taken as stationary, so the two terms on the extreme right in Eq. 16 can be neglected. From a computational perspective, to evaluate the flux from Eq. 15, one needs very accurate numerical estimation of the liquid-frac-

tion gradient at the lower foam boundary, necessitating dense packing of grid points close to ζ_b. This was accomplished by using a logarithmic grid in the numerical solution of the drainage equation.

Even a fully drained (equilibrium) foam preserves some liquid content, as a consequence of a balance between gravity and capillary gradient forces. The liquid fraction profile of equilibrium foam can be readily obtained by assuming no flow condition across the foam column and integrating with aid of the bottom boundary condition. This leads to the following:

$$\int_{\zeta_b}^{\zeta} d\zeta' = \int_{\varphi_b}^{\varphi_{eq}} \left(\varphi'^{-3/2}(1-\varphi')^{-1/2}\right) d\varphi', \qquad (17)$$

and

$$\varphi_{eq} = \left\{1+\left[\left(\frac{1-\varphi_b}{\varphi_b}\right)^{1/2} + \frac{1}{2}(\zeta_b - \zeta)\right]^2\right\}^{-1}. \qquad (18)$$

Equation (13), together with its initial and boundary conditions, was solved by using the finite-volume method (Patankar, 1980). The nonlinear terms were linearized and the solution was obtained by iteration. Usually, less than six iterations were needed at each time step to attain convergence, and no oscillatory behavior was observed during the iterations. Typical execution of the program requires less than 600 CPU s on a 300-MHz PC computer, for the liquid profile to evolve from the initial condition to the equilibrium solution. For more than a hundred grid points, the liquid holdup is insensitive to the number of grid points, but accurate drainage rate calculation requires additional grid points placed close to the foam's lower boundary.

The model also accounts for the fact that the foam layer is initially placed on a dry surface during the experiments, as demonstrated by Figure 3. This is achieved by imposing a no-flow boundary condition at the bottom until the liquid fraction reaches $\varphi_b = 0.26$, allowing the calculation of the time to the onset of drainage. Figure 3 shows the liquid-fraction profiles as function of foam height at short times: 0, 10, 40, 80, 160, and 240 s after generation. The foam ($\varphi_o = 0.05$) takes approximately 240 s before it begins to drain when placed on a dry surface (i.e., φ_b rises from 0.05 to 0.26 in 240 s). The time-to-drain will be used later in the article to estimate the value of the velocity coefficient c_v for the foams under study.

Finally, we observed that for a sufficiently dry foam placed on a layer of surfactant solution, the model predicts an initial flow of the solution into the foam layer (not studied experimentally in this article). This upward flow of the surfactant solution decays very rapidly with the arrival of the solution from the upper portion of the foam layer, leading to the onset of drainage.

Results and Discussion

In previous experimental studies (such as Sarma et al., 1988; Ramani et al., 1992; Hutzler et al., 1995; Koehler et al., 1999) on foam drainage, the foam was generated by air-aspiration,

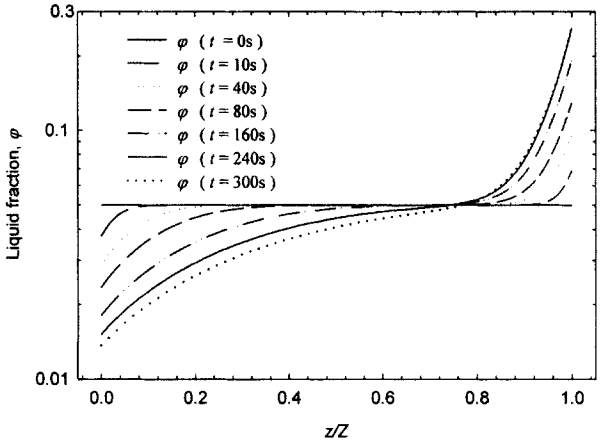

Figure 3. Liquid-fraction profiles as function of foam height at short times ($\varphi_o = 0.05$; $Z = 0.2$ m; $c_v = 4.5$; $r_{40} = 133$ μm).

The plot illustrates the modeling of the no-flow boundary condition when the foam is placed on a dry surface, and the onset of drainage.

and the liquid draining was allowed to accumulate below the foam layer. In contrast, we generate a foam column of uniform liquid fraction with height, and the liquid draining from the foam layer is allowed to flow out of the Perspex cylinder holding the foam column (i.e., the drained liquid is not allowed to accumulate below the foam layer). This is done in order to simulate a free-draining foam layer used for fire-fighting applications (Boyd and Dimarzo, 1998; Magrabi et al., 2000).

During the entire experiment, the foam column was covered with a moist cloth to prevent foam collapse due to evaporation. The top surface of the foam moved down over 3600 s by approximately 5–10 mm (2 to 5%) due to foam collapse. The presence of a 1–2-mm high liquid layer once the foam starts to drain allowed us to assume a critical liquid fraction ($\varphi = 0.26$) at the bottom of the foam column. This follows from the argument that the liquid fraction at this point corresponds to that for closed packed spheres, that is, $\varphi = 0.26$ (Bhakta and Ruckenstein, 1997).

Figure 4 shows the experimentally measured liquid fraction profiles for a foam ($\varphi_o = 0.05$) at $z/Z = 0.24$, 0.49, 0.81, and 0.91, respectively, where h is the height of interest in the foam column measured vertically downwards from the free foam surface, and H is the total height of the foam column. At any given height in the foam column, the local liquid fraction reflects the balance between the foam solution flowing in from above and the foam solution flowing out to the lower portion of the foam column, together with the accumulation or depletion of the foam solution. Initially, the foam column has a uniform liquid fraction throughout, but when drainage commences the foam at the top ($z/Z = 0$) becomes dry rapidly, as it does not receive any liquid from above. With time, a depletion profile develops, starting from the top and slowly moving toward the bottom of the foam layer. Finally, the liquid holdup at all heights in the column approaches a steady-state value, which represents the point at which the capillary and gravitational forces in the foam are in balance.

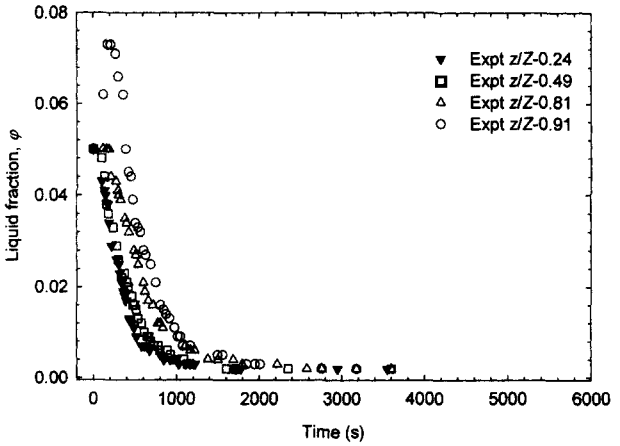

Figure 4. Liquid-fraction profiles measured by using the sonic-velocity method, as a function of time in a compressed-air foam ($\varphi_o = 0.05$).

The liquid-fraction profiles were measured at $z/Z = 0.24$, 0.49, 0.81, and 0.91, respectively.

As anticipated, the upper portions of the foam column (i.e., $z/Z = 0.24$) drain faster than the lower portions (i.e., $z/Z = 0.91$). The liquid fraction profile at $z/Z = 0.91$, which corresponds to a height roughly 10 mm from the base of the foam column, is different from the profiles measured at the higher positions in the foam column, exhibiting an initial rise in the liquid holdup followed by a decline. This occurs due to the initial accumulation of liquid draining from the upper portions of the foam column. A clear distinction in the drainage profiles at different heights was observed in the first 1800 s; subsequently the liquid fraction histories converged to almost the same value, as illustrated in Figure 4.

Figure 5 shows the results of the mass balance conducted on the foam column under study. It shows four experimental sets of the mass of foam solution drained from the foam column as a function of time ($\varphi_o = 0.05$). Inconsistencies with the initial amount of foam filled into the foam column led to

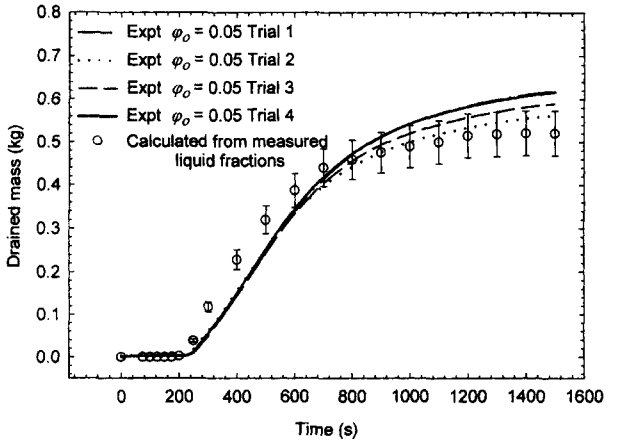

Figure 5. Mass-balance closure for the foam column under study ($\varphi_o = 0.05$).

A comparison of the directly measured drained mass and the drained mass calculated from the liquid-fraction profile measurements.

the experimental scatter observed in the drainage measurements. The points in Figure 5 were calculated from the experimentally measured liquid fraction profiles in Figure 4 by integrating the area under the curves and replotting the liquid fraction against the foam height at the desired times. The error bars represent the uncertainty of $\pm 10\%$ in the sonic velocity method. Good agreement is exhibited between the directly measured drained mass from the foam column and the drained mass calculated from the liquid-fraction measurements. This not only corroborates the closure of the mass balance on the foam column, but also establishes the accuracy of the sonic velocity method.

Two elementary types of film surfaces can be identified in foams on the basis of their thinning rates: mobile and rigid (Mysels et al., 1959). A fast thinning film surface is formed from most surfactants, as in the case of the aqueous foams generated from fluorocarbon surfactants in this study. On the other hand, rigid film surfaces are observed in protein foams (Germick et al., 1994; Wilde et al., 1999). The surface mobility of plateau borders and films is mainly dependent on the surface shear viscosity (or surface viscosity) and surface elasticity in the interfacial region. Foams with rigid film or plateau border surfaces have a no-slip boundary condition (i.e., $u = 0$) at the walls for the interfacial velocity, while foams with mobile film and plateau border surfaces have a slip boundary condition at the walls for the interfacial velocity (Steiner et al., 1977; Desai and Kumar, 1982; Joye et al., 1994).

Desai and Kumar (1982) have proposed the velocity coefficients c_v as a quantitative measure of the surface mobility of plateau borders or film walls. Here c_v is the ratio of the mean velocity through a film or plateau border when the surface viscosity is finite to the mean velocity when the surface velocity is infinite (i.e., rigid walls). More precisely, c_v is a function of the inverse of dimensionless surface shear viscosity, and hence has a value of unity for a foam with rigid film and plateau border walls ($c_v = 1$ gives $f = 144.1$ in Eq. 10). However, in foams with mobile interfaces, the no-slip boundary condition is no longer valid and the assumption of rigid interfaces in the drainage model severely underestimates the velocities in the channels. In this case, c_v could be calculated from surface-viscosity measurements, as suggested by Desai and Kumar (1982).

The surface viscosity in the interfacial region is greatly influenced by the blend of surfactants used and has been reported to vary over several orders of magnitude (Shah et al., 1978; Danov et al., 1999). The unavailability of surface-viscosity data in the literature for the present solution of fluorocarbon surfactants necessitated alternative means of estimating c_v. As as initial estimate, the surface viscosity $\mu_s = 1 \times 10^{-7}$ kg·s^{-1} for a 0.01% sodium lauryl sulphate (Kanner and Glass, 1969) was used to calculate c_v, which was estimated to be approximately 1.74. However, due to the higher surface mobility (i.e., lower surface viscosity) induced by fluorocarbon surfactants in the interfacial regions, c_v was expected to be substantially higher for the surfactant solution used in this work. Figure 6 demonstrates the sensitivity of the modeled liquid fraction contours to c_v as a function of time. As c_v is increased reflecting the slip at the plateau border walls, the drainage is substantially enhanced.

In this article, the velocity coefficient c_v was indirectly estimated by experimentally measuring the time taken for the

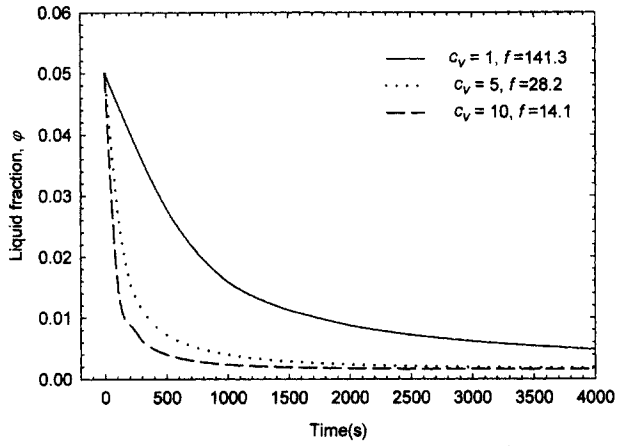

Figure 6. Effect of the velocity coefficient c_v on the simulated drainage profiles in a foam (φ_o = 0.05) at z/Z = 0.5, where c_v is taken as unity in foams with rigid film and plateau border walls.

foam solution to start draining (time-to-drain) once the foam column is generated. The time-to-drain is subsequently used in the drainage simulation as a modeling parameter to iterate for the velocity coefficients c_v. Figure 7 shows the measured time-to-drain for foams in the liquid-fraction range φ_o = 0.033–0.1, varying from 293 s for the foam (φ_o = 0.033) to 141 s for the foam (φ_o = 0.1). As anticipated, the larger the liquid fraction in the foam, the quicker the foam reaches the stage when it begins to drain.

Figure 7 also shows the velocity coefficient c_v obtained by adjusting the model to fit the time-to-drain data. The time-to-drain, the fill-time, and the velocity coefficients for foams in the φ_o = 0.033–0.1 range are listed in Table 1. The fill-time denotes the time taken to fill the holding container, to produce a foam column of desired liquid fraction and dimensions (0.2 m high by 0.29 m diameter). The time-to-drain and

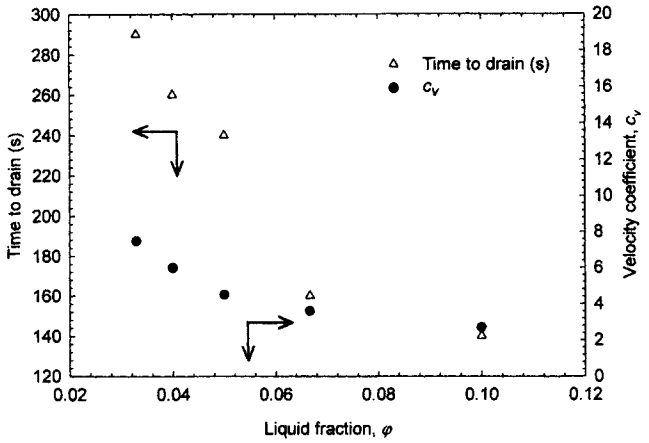

Figure 7. Velocity coefficient c_v and time-to-drain as a function of the liquid fraction, where c_v and time-to-drain increase with decreasing liquid fraction in the foam.

Table 1. Time-to-Drain, Fill-Times, and Velocity Coefficients for Foams of Varying Liquid Fraction (φ_o = 0.033–0.1)

Liquid Fraction φ_o	Time-to-Drain (s)	Fill Time (s)	Velocity Coefficient, c_v
0.1	141	85	2.7
0.067	162	88	3.6
0.05	240	70	4.5
0.04	258	41	6
0.033	293	36	7.5

fill-times are recorded on the same time scale (same origin, t = 0). It was found that c_v increases with decreasing liquid fraction, which follows from the argument that the drier the foam, the longer the channels and the greater the effects of slip at the plateau border walls on drainage. Since c_v was calculated from drainage measurements rather than from fundamental measurements of surface viscosity, it is considered an adjustable parameter.

Figure 8 shows a comparison between the modeled and experimentally measured liquid fraction profiles in a foam (φ_o = 0.05) at z/Z = 0.24, 0.49, 0.81, and 0.91, respectively. The drainage was simulated using the initial bubble size r_{40} = 133 μm and the velocity coefficient c_v = 4.5 (see Table 1). The mean bubble radius given by the fourth moment r_{40} was used in the drainage model as a representation of the characteristic bubble size in the foam column. A justification for this is presented in Appendix B. Figure 8 illustrates a reasonable agreement between the modeled and experimental drainage profiles for all sections of the foam column, but only during the initial 200 s. The discrepancy between the simulated and experimental data after 200 s can be attributed to the fact that the drainage equation (Eq. 13) does not consider the effects of foam coarsening due to interbubble gas diffusion, and strictly applies to fast-draining foams where drainage takes place much faster than coarsening. In addition, after the initial 200 s, wider disparities between the

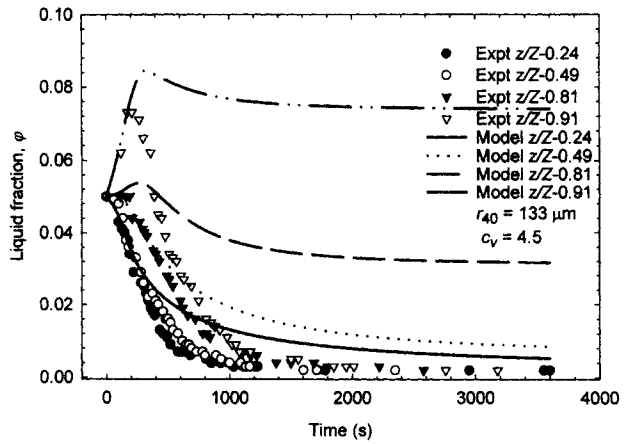

Figure 8. Modeled vs. experimentally measured liquid-fraction profiles in a foam column (φ_o = 0.05; Z = 0.2 m; c_v = 4.5; initial bubble size r_{40} = 133 μm) at z/Z = 0.24, 0.49, 0.81, and 0.91, respectively.

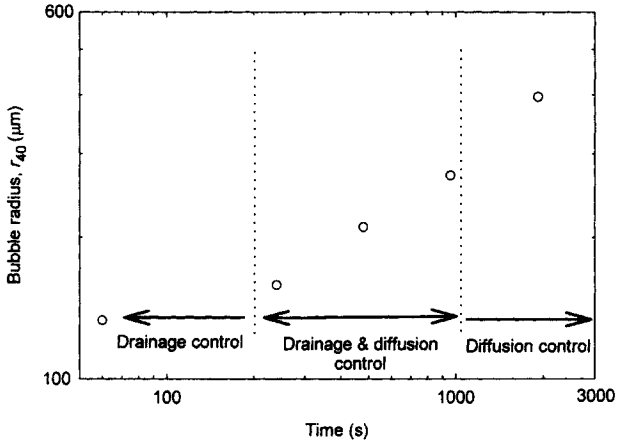

Figure 9. Bubble growth in compressed-air foams (φ_o = 0.05).

In the first 200 s, drainage is more dominant than coarsening and takes place on a faster time scale; subsequently after 200-s drainage and coarsening occur on a concurrent time scale; and finally after 960-s coarsening prevails over drainage.

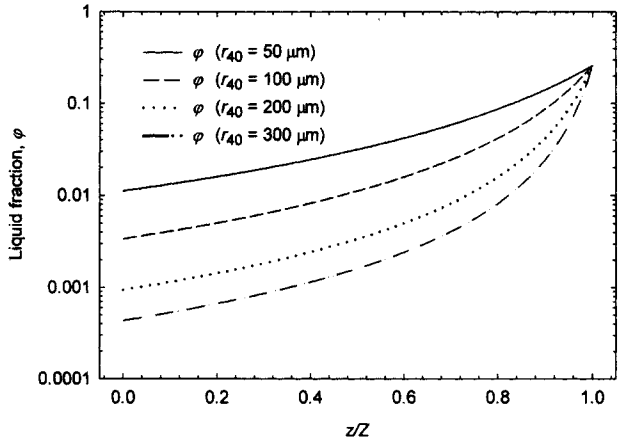

Figure 10. Effect of bubble size r_{40} on the modeled equilibrium liquid-fraction profiles (φ_o = 0.05; Z = 0.2 m; c_v = 4.5).

Foams with larger bubbles have drier equilibrium liquid profiles.

modeled and experimental data were observed in the lower portions of the foam column ($z/Z = 0.81$ and 0.91) than in the upper sections ($z/Z = 0.24$ and 0.49). This is interpreted in the following sections of this article.

Figure 9 demonstrates that foam bubbles ($\varphi_o = 0.05$) of initial radius $r_{40} = 133$ μm, can almost double in size to $r_{40} = 270$ μm in 960 s, but they really start to grow rapidly after about 200 s. In the first 200 s, drainage is more dominant than coarsening and takes place on a faster time scale; subsequently, after 200 s drainage and coarsening occur on a comparable time scale; and finally after 960 s coarsening prevails over drainage. In contrast to previous work by the authors (Magrabi et al., 1999), where the transition from drainage to drainage coupled with diffusion was reported at 500 s, the present results indicate that the latter transition occurs at 200 s in the current experiments. Consequently, based on the present data the transition boundary from drainage to drainage coupled with diffusion is lowered to 200 s.

Figure 10 illustrates the effect of the bubble size r_{40} on the modeled equilibrium liquid profiles. For larger bubbles, the equilibrium liquid fraction profile is drier than for smaller bubbles. As a consequence of the growth of larger bubbles and disappearance of small bubbles due to interbubble diffusion, the foam coarsens, leading to additional outflow of surfactant solution. Accordingly, we denote this phenomenon as coarsening-induced drainage.

Figure 11 illustrates the effect of using a larger bubble size in the drainage model. Drainage from the foam column was simulated using the bubble size $r_{40} = 270$ μm at 960 s and $c_v = 4.5$, as shown in Figure 9. In Figure 11, the model predictions show excellent agreement with the experimental drainage profiles after 960 s at $z/Z = 0.24$ and 0.49, as the model utilizes the bubble size at 960 s, $r_{40} = 270$ μm. Hence, we can conclude that excellent conformity is exhibited in the upper and middle sections of the foam column. However, there is a discrepancy between the modeled and measured data in the lower section of the foam. It should be noted that c_v was kept constant at 4.5 during the entire simulation and for the purpose of this calculation was not considered to be a function of φ, as indicated in Figure 7.

A comparison of Figures 8 and 11 shows a clear distinction in the time required to reach equilibrium, with the coarser foam $r_{40} = 270$ μm reaching equilibrium faster than the finer foam $r_{40} = 133$ μm. As illustrated in Figure 10, foams with larger bubbles have drier equilibrium profiles due to the larger cross-sectional area of plateau borders and the gentler gradient of capillary pressure across the foam column, which in turn produce larger drainage rates. With reference to Figures 8 and 11, the current model can adequately predict the liquid-fraction profiles in the upper and middle sections ($z/Z = 0.24$ and 0.49) of the foam column in the first 200 s and

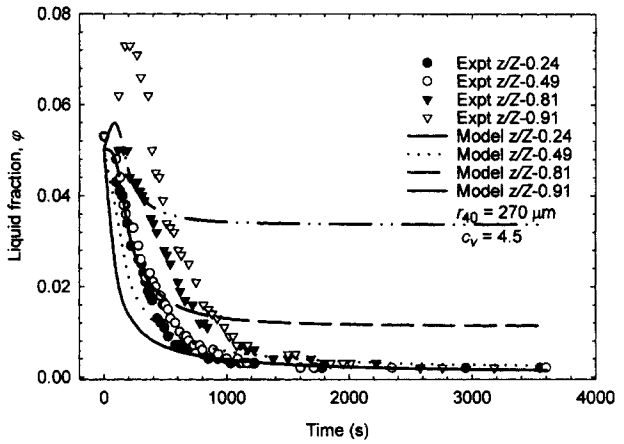

Figure 11. A comparison of the modeled and experimentally measured liquid-fraction profiles in a foam column using the bubble size r_{40} = 270 μm at 960 s (φ_o = 0.05; Z = 0.2 m; c_v = 4.5) at h/H = 0.24, 0.49, 0.81, and 0.91, respectively.

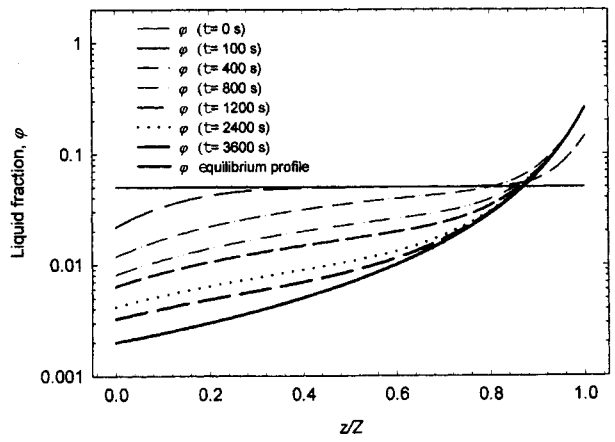

Figure 12. Liquid profiles with time as function of foam height ($\varphi_o = 0.05$; $Z = 0.2$ m; $c_v = 4.5$; $r_{40} = 270$ μm).

After 1200 s, the foam height $z/Z \approx 0.87$ signifies the critical elevation at which the liquid fraction is the same as the initial liquid fraction, in this case $\varphi_o = 0.05$.

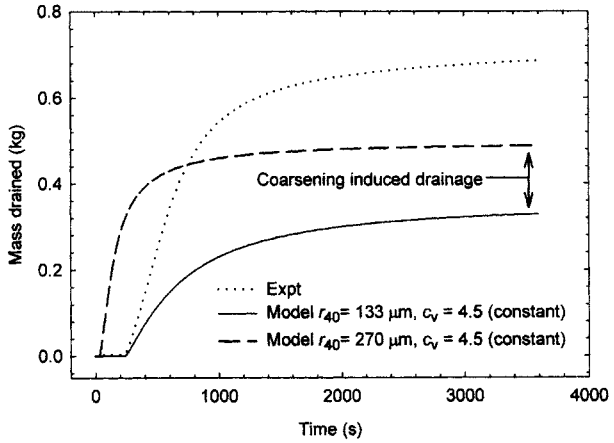

Figure 13. Effect of bubble size on the simulated drainage from a foam column ($\varphi_o = 0.05$; $Z = 0.2$ m; $c_v = 4.5$).

The plot compares the experimental drainage measurements with the simulations using the initial bubble size $r_{40} = 133$ μm and the bubble size at 960 s, $r_{40} = 270$ μm, and demonstrates coarsening-induced drainage.

after 960 s, when the transient bubble size r_{40} is incorporated into the simulation. In the lower portions of the foam column ($z/Z = 0.81$ and 0.91), the model gives fair agreement with the experimental determination in the initial 200 s. Furthermore, the model accurately predicts the initial rise in liquid fraction observed at $z/Z = 0.81$ and 0.91. However, in Figures 8 and 11 the equilibrium liquid-fraction profiles at $z/Z = 0.24$ and 0.49 were much higher than experimental observations. A possible rationale for this could be the accumulation of liquid at the bottom of the foam column during the simulation. The latter occurs due to the boundary condition imposed by the model at the lower end of the foam column, which corresponds to that of closed-packed spheres at the foam–liquid interface, $\varphi_b = 0.26$ at $z = 0.2$ m.

Figure 12 is essentially an extension of Figure 3 and illustrates the liquid-fraction profiles as a function of foam height at longer times. The plot elucidates the effect of the closed-packed sphere boundary condition and the transient drainage profiles in $\varphi_o = 0.05$ foam at $t = 0$, 100, 400, 800, 1,200, and 3,600 s and at equilibrium. In the initial 200 s, the liquid holdup rises very rapidly in the lower part of the foam column to reflect the bottom boundary condition. The drainage starts at approximately 240 s with the arrival of additional surfactant solution from the upper portions of the foam column, as manifested by Figure 3. The liquid holdup changes significantly in all portions of the foam column in the first 1,200 s. In the following period, the liquid holdup shows very small changes as the foam tends to equilibrium.

In the lower sections of the foam column (such as $z/Z = 0.91$), the model allows for the liquid fraction to rise and then drop, as illustrated in Figures 8 and 11. After 1,200 s, the foam height $z/Z \approx 0.87$ signifies the critical elevation at which the liquid fraction is the same as the initial liquid fraction, in this case $\varphi_o = 0.05$. The foam at this height reaches the initial liquid fraction $\varphi_o = 0.05$ after approximately 1,200 s and retains this liquid fraction until equilibrium is attained. Similarly, constant liquid holdup was exhibited by the modeled predictions at all portions of the foam below $z/Z \approx 0.87$, as shown in Figure 12. Physically, the latter was not observed in the experiments and arose in the simulations as a consequence of the boundary condition used in the model at the lower surface. It is also possible that our model does not capture some essential, but yet unknown characteristics of the system close to the lower boundary, ζ_b, including coarsening that was not incorporated in this model. The experiments plotted in Figure 4 show that the foam reaches equilibrium, $\varphi \approx 0.001$, at all elevations in the column. It should be noted, however, that $\varphi \approx 0.001$ corresponds to the lower limit of the sonic velocity method. Thus, Figure 12 demonstrates the strong dependence of the modeled liquid-fraction contours on the chosen lower boundary condition. In the later sections of this article, we review alternative lower boundary conditions that have been suggested in the literature.

Liquid drainage from the foam column ($\varphi_o = 0.05$) is shown in Figure 13. Drainage was simulated by using the initial bubble size $r_{40} = 133$ μm and the bubble size at 960 s of $r_{40} = 270$ μm. The velocity coefficient c_v was kept constant at $c_v = 4.5$, during the entire simulation in both the latter cases. Equation 15 gives the modeled mass flux draining from the foam column. As in the case of the liquid-fraction predictions in Figures 8 and 11, there is initial agreement between the modeling and experiments followed by a disparity between the model predictions and the experimental data at later times. Figure 13 also shows the influence of coarsening-induced drainage in foams. As the foam coarsens from $r_{40} = 133$ μm to $r_{40} = 270$ μm, there is an increase in the rate of drainage from the column, primarily due to the additional outflow of surfactant solution from the disappearance of small bubbles and the growth of larger ones.

Similarly, Figure 14 compares the experimental and modeled drainage rates from the foam column ($\varphi_o = 0.05$, $Z = 0.2$ m, $c_v = 4.5$) for different bubble sizes. The model shows a similar drainage trend to the experiments, with a dramatic rise followed by a gradual decline. The application of the initial bubble radius $r_{40} = 133$ μm in the simulation gives an

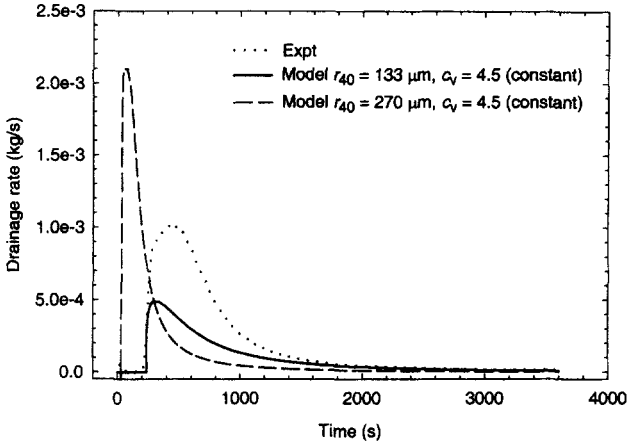

Figure 14. Drainage rate from the foam column (φ_o = 0.05; Z = 0.2 m; c_v = 4.5).

A comparison between the modeled and experimental drainage rates from the foam column.

accurate prediction of the drainage rate for the first 200 s. Subsequently, the absence of coarsening in the model causes a discord with the experiments in the later stages. Using the bubble size at 960 s of $r_{40} = 270$ μm in the model causes the drainage rate to rise dramatically in the first 200 s. This is followed by a rapid decline due to the inability of the foam column to sustain the large drainage rates warranted by the bubble growth as a consequence of coarsening. Furthermore, this demonstrates the influence of coarsening-induced drainage on the total amount of foam solution discharged by a foam column.

Limitations of the Current Drainage Model

Figures 8, 11, 13 and 14 clearly demonstrate that the liquid fraction profiles, drainage rates, time-to-drain, final equilibrium profiles, and the time to attain equilibrium predicted by the drainage model are strongly dependent on the bubble size used in the simulation. Thus, improved conformity between the experiments and drainage model could be achieved by incorporating coarsening (i.e., transient bubble size) into the model, for instance, by coupling the model developed by Magrabi et al. (1999) for coarsening with the present drainage model. However, this was not attempted in the present article.

Due to the absence of coarsening in this drainage model, an appropriate bubble size was required to represent the transient bubble size in the foam column. In their study, Germick et al. (1994) utilized a characteristic bubble size, which was reported to be different from the mean bubble size, to model their experimental foam bed. Instead of using the bubble size as a fitted parameter, we simulated foam drainage using c_v as an adjustable parameter derived from experiments and the actual bubble size r_{40} in order to highlight any limitations in the model.

By using the mean initial bubble size r_{40}, a reasonable agreement was demonstrated between the modeling and experiments for the initial 200 s, as illustrated by Figures 8, 13, and 14. Moreover, Figures 11, 13, and 14 show that by using $r_{40} = 270$ μm at 960 s, a good agreement between the simulated and the experimental investigations at $z/Z = 0.24$ and 0.49 was apparent after 960 s. Finally, by virtue of simulating our experimental observations using bubble sizes at two time instances to expound the significance of coarsening, we have shown the drawbacks of excluding Ostwald ripening from a drainage model. This was not very apparent in previous foam drainage studies.

The drainage equation (Eq. 13) used in the modeling assumes a no-slip boundary condition (i.e., rigid walls, $v = 0$) in the films and plateau borders. In order to incorporate the surface mobility of the plateau border and film walls, a velocity coefficient c_v was introduced that varied with liquid faction (see Figure 7 and Table 1). Recently, Koehler et al., (1999) proposed an alternative approach to viscous dissipation in the foam drainage model. It emphasizes the importance of viscous damping in the nodes or vertices (i.e., regions where four plateau borders meet) together with the relaxation of the wall rigidity in the plateau borders themselves. This introduces a pluglike flow in the plateau borders with dissipative shear flow occurring only within the vertices. The model predictions using the latter approach showed improved agreement for forced drainage experiments, where the speed of a liquid front advancing in a dry foam column in a narrow tube geometry (length = 1.5 m, diameter = 0.025 m) was studied (Koehler et al., 1999).

The extent to which vertex dissipation becomes significant is largely dependent on the liquid fraction of the foam. In a wet foam (such as $\varphi_0 = 0.2$), it is expected that vertex dissipation becomes significant due to the expansion of the nodes as a result of the larger liquid holdup. In a relatively dry foam (such as $\varphi_0 = 0.05$), however, the longer plateau borders will result in channel-dominated dissipation. In this study, the variation in viscous dissipation with liquid fraction has been accounted for by Figure 7, where the surface viscosity in the channels is inversely proportional to the liquid fraction (i.e., $c_v \propto 1/\varphi$). The inclusion of vertex dissipation in the model will further reduce the simulated drainage rates. In general, the current model predicted slower drainage rates than the experimental observations, hence, the inclusion of vertex dissipation will cause wider disparity. However, our study showed that foam coarsening by far has a more profound effect on the model predictions than the viscous dissipation.

The current drainage model assumes that the foam solution in the plateau borders has no inertia, in that the inertial terms in the equation of motion, which would appear on the right of Eq. 2, have been set identically to zero. This assumption is not entirely true, as the liquid in the films and channels possesses inertia and the flow has to be accelerated to start drainage from the column. In addition, the cross-sectional area of the channel walls continuously changes with time, resulting in the evolution of the parabolic liquid flow profile. This gives a quasi-steady-state flow rather than the steady-state flow assumed in this model. By assuming the quasi-steady-state assumption, the present model implies that the parabolic liquid flow profile in the channels is established on a faster time scale than drainage.

The drainage model used in this analysis considers the drainage through plateau borders while neglecting film drainage altogether. The addition of film drainage in the

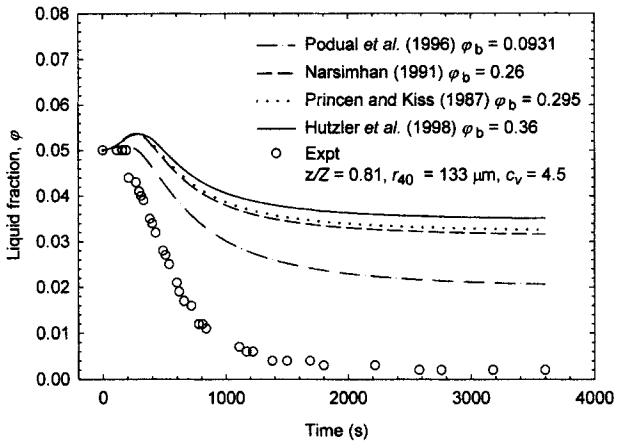

Figure 15. Sensitivity of the drainage model to the lower boundary condition ($\varphi_o = 0.05$; $Z = 0.2$ m; $c_v = 4.5$).

The plot illustrates the modeled liquid-fraction predictions at $z/Z = 0.81$ using various φ_b reported in the literature.

model will further accelerate the drainage process (Ramani et al., 1992; Gururaj et al., 1995). However, the effect of the latter is expected to be insignificant in comparison to the effect of coarsening.

The boundary condition used at the bottom of the foam column (i.e., $z/Z = 1$) was found to strongly influence the model predictions, as illustrated by Figure 15. The existing condition of $\varphi_b = 0.26$ is a good first approximation of the foam–liquid interface where the bubbles touch the liquid pool below them, and provides the closest replication of the bubble packing seen in our experiments. Although this condition has been utilized in many studies previously (Narsimhan, 1991; Germick et al., 1994; Bhakta and Ruckenstein, 1997), it is not an entirely accurate description of the experimental boundary condition.

Several other boundary conditions at the foam–liquid interface have been reported in the literature. Podual et al. (1996) reported that close-packed cylinders appeared to be a better assumption than close-packed spheres at the bottom boundary and used $\varphi_b = 0.0931$. Princen and Kiss (1987) observed that the emulsion droplets do not pack as efficiency as identical spheres because of the distribution of emulsion drop sizes and measured the liquid fraction at the emulsion–liquid interface as $\varphi_b = 0.295$. Hutzler et al. (1998) reported that the liquid fraction at the bottom boundary corresponds to the space between the random packing of spheres, as in Bernal packing, $\varphi_b = 0.36$. Saint-Jalmes et al. (1999) have suggested an almost identical value to the latter, $\varphi_b = 0.37$. Although the model prediction using the lower boundary condition suggested by Podual et al. (1996), $\varphi_b = 0.0931$, showed the closest conformity to the experimental measurements, the latter was not utilized, as it was not compliant with the bubble packing observed during our experiments. The other boundary conditions suggested by Princen and Kiss (1987), Hutzler et al. (1998), and Saint-Jalmes et al. (1999) give higher equilibrium liquid-fraction profiles and show greater disagreement with experiments, as shown by Figure 15.

Conclusions

This article presents experimental and theoretical studies of free drainage in compressed-air foams. The time evolution of liquid-fraction profiles in a 0.2-m-high by 0.29-m-diameter foam column was measured at various heights by using the sonic velocity method. A new experimental technique was devised in this article to measure the true drainage rate of surfactant solution leaving the foam column.

A new form of the drainage equation has been developed describing the holdup of surfactant solution in the foam directly in terms of the liquid-fraction profile. The present equation formulates the drainage problem in terms of liquid fraction, which is of practical interest and can be measured directly with ease. Furthermore, by using this formulation, the drainage equation can be used to predict the discharge rate of foam solution from foam columns.

In order to account for the surface mobility at the plateau border and film walls, induced by the blend of fluorocarbon surfactants used in this study, the time taken for the foam solution to start draining once the foam column is generated was experimentally measured. The time-to-drain was subsequently used in the drainage simulation as a modeling parameter to iterate for the velocity coefficient, c_v, which was found to increase with decreasing liquid fraction.

The model applies with one adjustable parameter (i.e., c_v), to predict drainage from foams containing mobile plateau border and film walls. The liquid-fraction contours, drainage rates, time-to-drain, final equilibrium liquid profiles, and the time to attain equilibrium predicted by the model are strongly dependent on the bubble size used in the simulation. The mean bubble size given by the fourth moment of the bubble radius, r_{40}, was found to be the most appropriate bubble size to apply in the drainage model. Significantly, the model does not use the bubble size as an adjustable parameter.

Interbubble gas diffusion in foams leads to the growth of larger bubbles at the expense of smaller ones. The phenomenon resulting in the additional outflow of surfactant solution from the extinction of small bubbles is denoted in this article as coarsening-induced drainage. Over extended time periods, the present model needs to be coupled with interbubble gas diffusion in order to incorporate coarsening-induced drainage.

The following factors have significant bearing on the drainage predictions in decreasing order of magnitude: the lack of coarsening; the boundary condition at the foam–liquid interface at the bottom of the foam column; the assumption of zero inertia as well as the absence of film drainage and vertex dissipation. From this standpoint, we remark that foam-drainage and coarsening processes are intimately coupled, necessitating the development of new models. These models should be able to provide a more realistic and precise foam-drainage profile by being able to predict coarsening-induced drainage, which is important at longer drainage times.

Acknowledgments

The authors acknowledge Mr. Robin D'Ombrain for his assistance in the development of the sonic-velocity method and the drainage measurement techniques. This study was funded by the Australian Research Council, by a student grant from the Society of Fire Pro-

tection Engineers (SFPE), with additional support from the Centre for Multiphase Processes.

Notation

a_p = cross-sectional area of a plateau border channel, m^2
b = averaging constant for pentagonal dodecahedra bubble structure, 3/15
C_p = specific heat capacity at constant pressure, $J \cdot kg^{-1} \cdot K^{-1}$
C_v = specific heat capacity at constant volume, $J \cdot kg^{-1} \cdot K^{-1}$
c_v = velocity coefficient, function of the dimensionless surface viscosity
e = constant, 0.816 for pentagonal dodecahedra
f = supplementary constant defined in Eq. 10
g = gravitational constant, 9.81 $m \cdot s^{-2}$
l = length of a channel, $l = er$, m
N = number of bubbles per unit volume, m^{-3}
n_p = number of channels per bubble (10, for pentagonal dodecahedra)
P_a = atmospheric pressure, Pa
p = pressure in plateau borders, Pa
p_b = pressure in bubbles, Pa
q''_b = nondimensional variable corresponding to the rate of foam solution drained per cross section of foam column
r = radius of a sphere whose volume equals volume of a foam cell, m
r_{40} = mean radius defined by the fourth moment, m
r_c = radius of curvature of a channel wall, m
t_o = constant defined in Eq. 11, s
u = velocity of foam solution in a plateau border, $m \cdot s^{-1}$
V = bubble volume, m^3
v = average velocity of foam solution in a plateau border, $m \cdot s^{-1}$
v_{sf} = sonic velocity in foam, $m \cdot s^{-1}$
Z = height of the foam column, m
z = height of interest in the foam column, downward from the free surface, m
z_o = constant defined in Eq. 12, m

Greek letters

δ = constant equal to $(3^{1/2} - (\pi/2))$
γ = ratio of specific heat capacities $\gamma = C_p/C_v$
φ = liquid fraction
φ_b = liquid fraction at the bottom of foam column (0.26)
φ_{eq} = equilibrium liquid fraction
φ_o = initial uniform liquid fraction
μ = viscosity of the surfactant solution (8.93×10^{-4} Pa·s)
μ_s = surface shear viscosity or surface viscosity in the interfacial region, $kg \cdot s^{-1}$
ρ = density of the surfactant solution (997 $kg \cdot m^{-3}$)
σ = surface tension of the surfactant solution (22.5×10^{-3} $N \cdot m^{-1}$)
τ = nondimensional time coordinate
ξ = nondimensional spatial coordinate
ζ_b = location of the interface between foam and surfactant solution

Literature Cited

Bhakta, A., and E. Ruckenstein, "Drainage of Standing Foam," *Langmuir*, **11**, 1486 (1995).

Bhakta, A., and E. Ruckenstein, "Decay of Standing Foams–Drainage, Coalescence and Collapse," *Adv. Coll. Int. Sci.*, **70**, 1 (1997).

Boyd, C. F., and M. Dimarzo, "The Behaviour of a Fire-Protection Foam Exposed to Radiant Heating," *Int. J. Heat Mass Transfer*, **41**, 1719 (1998).

Danov, K. D., D. S. Valkovska, and I. B. Ivanov, "Effect of Surfactants on the Film Drainage," *J. Coll. Int. Sci.*, **211**, 291 (1999).

Desai, D., and R. Kumar, "Flow Through a Plateau Border of Cellular Foam," *Chem. Eng. Sci.*, **37**, 1361 (1982).

Fortes, M. A., and S. Coughlan, "Simple Model of Foam Drainage," *J. Appl. Phys.*, **76**, 4028 (1994).

Gardiner, B. S., B. Z. Dlugogorski, and G. J. Jameson, "Rheology of Fire-Fighting Foams," *Fire Safety J.*, **31**, 61 (1998a).

Gardiner, B. S., B. Z. Dlugogorski, and G. J. Jameson, "Yield Stress Measurements of Foams," *J. Rheol.*, **42**, 1437 (1998b).

Germick, R. J., A. S. Rehill, and G. Narsimhan, "Experimental Investigation of Static Drainage of Protein Stabilised Foams—Comparison with Model," *J. Food Eng.*, **23**, 555 (1994).

Goldfarb, I. I., K. B. Kann, and I. R. Shreiber, "Liquid Flow in Foams," *Fluid Dynamics (Trans. USSR Acad. Sci., Mechanics of Liquid and Gas Series)*, **23**, 244 (1988).

Goldshtein, V., I. Goldfarb, and I. Schreiber, "Drainage Waves Structure in Gas-Liquid Foam," *Int. J. Multiphase Flow*, **22**, 991 (1996).

Gururaj, M., R. Kumar, and K. S. Gandhi, "A Network Model of Static Foam Drainage," *Langmuir*, **11**, 1381 (1995).

Hutzler, S., G. Verbist, D. Weaire, and J. A. Van Der Steen, "Measurement of Foam Density Profiles Using AC Capacitance," *Europhys. Lett.*, **31**, 497 (1995).

Hutzler, S., D. Weaire, and R. Crawford, "Convective Instability in Foam Drainage," *Europhys. Lett.*, **41**, 461 (1998).

Isaksson, S., and H. Persson, "Fire Extinguishing Foam—Test Method for Heat Exposure Characterisation," SP Rep. 1997:09, Swedish National Testing and Research Institute, Boras (1997).

Joye, J., G. J. Hirasaki, and C. A. Miller, "Asymmetric Drainage in Foam Films," *Langmuir*, **10**, 3174 (1994).

Kanner, B., and E. J. Glass, "Surface Viscosity and Elasticity: Significant Parameters in Industrial Processes," *Ind. Eng. Chem.*, **61**, 31 (1969).

Koehler, S. A., S. Hilgenfeldt, and H. A. Stone, "Liquid Flow Through Aqueous Foams: The Node-Dominated Foam Drainage Equation," *Phys. Rev. Lett.*, **82**, 4232 (1999).

Koehler, S. A., H. A. Stone, M. P. Brenner, and J. Eggers, "Dynamics of Foam Drainage," *Phys. Rev. E*, **58**, 2097 (1998).

Magrabi, S. A., B. Z. Dlugogorski, and G. J. Jameson, "Bubble Size Distribution and Coarsening in Aqueous Foams," *Chem. Eng. Sci.*, **54**, 4007 (1999).

Magrabi, S. A., B. Z. Dlugogorski, and G. J. Jameson, "The Performance of Aged Aqueous Foams in the Mitigation of Thermal Radiation," *Dev. Chem. Eng. Min. Proc. J.*, **8**, 93 (2000).

Manasseh, R., "Acoustic Sizing of Bubbles at Moderate to High Bubbling Rates," *Experimental Heat Transfer, Fluid Mechanics and Thermodynamics*, Edizioni ETS, Pisa, p. 943 (1997).

Mysels, K. J., K. Shinoda, and S. Frankel, *Soaps Films: Studies of Their Thinning and a Bibliography*, Pergamon, Oxford (1959).

Narsimhan, G., "A Model of Unsteady State Drainage of a Static Foam," *J. Food Eng.*, **14**, 139 (1991).

Narsimhan, G., and E. Ruckenstein, "Effect of Bubble Size Distribution on the Enrichment and Collapse in Foams," *Langmuir*, **2**, 494 (1986).

Patankar, S. V., *Numerical Heat Transfer and Fluid Flow*, Hemisphere, New York (1980).

Persson, H., "Fire Extinguishing Foams—Resistance Against Heat Resistance," SP Rep. 1992:54, Swedish National Testing and Research Institute, Boras (1992).

Podual, K., R. Kumar, and K. S. Gandhi, "A New Model for Drainage of Static Foams," *Chem. Eng. Sci.*, **51**(9), 1393 (1996).

Princen, H. M., and A. D. Kiss, "Osmotic Pressure of Foams and Highly Concentrated Emulsions: 2. Determination from the Variation in Volume Fraction with Height in an Equilibrated Column," *Langmuir*, **3**, 36 (1987).

Ramani, M. V., R. Kumar, and K. S. Gandhi, "A Model for Static Foam Drainage," *Chem. Eng. Sci.*, **48**, 455 (1992).

Saint-Jalmes, A., M. U. Vera, and D. J. Durian, "Uniform Foam Production by Turbulent Mixing: New Results on Free Drainage vs. Liquid Content," *Eur. Phys. J. B*, **12**, 67 (1999).

Sarma, S. R., J. Pandit, and K. C. Khilar, "Enhancement of Stability of Aqueous Foams by Addition of Water Soluble Polymers—Measurements and Analysis," *J. Colloid Interface Sci.*, **124**, 339 (1988).

Shah, D. O., N. F. Djabbarah, and D. T. Wasan, "A Correlation of Foam Stability with Surface Shear Viscosity and Area per Molecule in Mixed Surfactant Systems," *Coll. Polym. Sci.*, **256**, 1002 (1978).

Steiner, L., R. Hunkeler, and S. Hartland, "Behaviour of Dynamic Cellular Foams," *Trans. Inst. Chem. Eng.*, **55**, 153 (1977).

Verbist, G., D. Weaire, and A. Kraynik, "The Foam Drainage Equation," *J. Phys. Cond. Mater.*, **8**, 3715 (1996).

Wilde, P. J., A. R. Mackie, F. A. Husband, A. P. Gunning, V. J. Morris, and A. Fillery-Travis, "Foams and Films," *Int. Workshop on Foams and Films*, MIT Publishing, Cambridge, MA, p. 59 (1999).

Wood, A. B., *A Textbook of Sound*, Bell, London (1941).

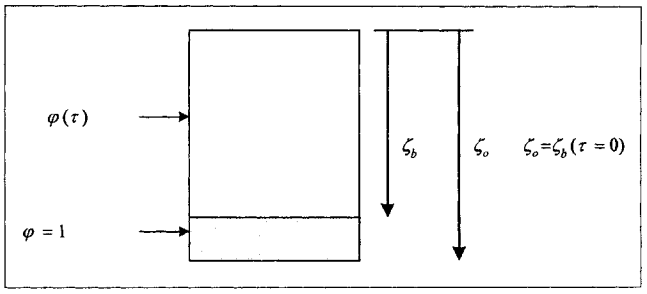

Figure A1. Draining foam column.

Appendix A: Calculation of the Foam–Liquid Interface in a Draining Foam

With reference to Figure A1, the mass balance for a draining foam column can be written as

$$\underbrace{\int_0^{\zeta_0} \varphi_0 \, d\zeta}_{\substack{\uparrow \\ \text{Solution initially in the foam}}} = \underbrace{\int_0^{\zeta_b(\tau)} \varphi(\tau) \, d\zeta}_{\substack{\uparrow \\ \text{Solution in the foam at time } \tau}} + \underbrace{\int_{\zeta_b(\tau)}^{\zeta_0} 1 \cdot d\zeta}_{\substack{\uparrow \\ \text{Solution drained from the foam at time } \tau}} \tag{A1}$$

$$\int_0^{\zeta_0} \varphi_0 \, d\zeta - \zeta_0 = \int_0^{\zeta_b(\tau)} \varphi(\tau) \, d\zeta - \zeta_b(\tau). \tag{A2}$$

Differentiating Eq. A2 gives

$$0 = \frac{d}{d\tau} \int_0^{\zeta_b(\tau)} \varphi(\tau) \, d\zeta - \frac{d\zeta_b(\tau)}{d\tau}. \tag{A3}$$

Applying the Leibnitz rule for differentiation of integrals and solving for ζ_b results in the following (Bhakta and Ruckenstein, 1995):

$$0 = \varphi_b \frac{d\zeta_b}{d\tau} + \int_0^{\zeta_b(\tau)} \frac{\partial \varphi}{\partial \tau} d\zeta - \frac{d\zeta_b}{d\tau} \tag{A4}$$

$$(1-\varphi_b)\frac{d\zeta_b}{d\tau} = -\int_0^{\zeta_b(\tau)} \frac{\partial}{\partial \zeta} \underbrace{\left(\frac{\varphi^2}{1-\varphi} - \frac{\varphi^{1/2}}{(1-\varphi)^{3/2}} \frac{\partial \varphi}{\partial \zeta} \right)}_{\text{from Eq. 13}} d\zeta \tag{A5}$$

$$(1-\varphi_b)\frac{d\zeta_b}{d\tau} = -\left(\frac{\varphi_b^2}{1-\varphi_b} - \frac{\varphi_b^{1/2}}{(1-\varphi_b)^{3/2}} \left. \frac{\partial \varphi}{\partial \zeta} \right|_{\zeta_b} \right) \tag{A6}$$

$$\int_{\zeta_0}^{\zeta_b(\tau)} d\zeta_b = \int_0^{\tau} \left(-\frac{\varphi_b^2}{(1-\varphi_b)^2} + \frac{\varphi_b^{1/2}}{(1-\varphi_b)^{5/2}} \left. \frac{\partial \varphi}{\partial \zeta} \right|_{\zeta_b} \right) d\tau'. \tag{A7}$$

The location of the interface between the foam and surfactant solution ζ_b as a function of time is given by the following expression:

$$\zeta_b(\tau) = \zeta(\tau = 0) - \frac{\varphi_b^2}{(1-\varphi_b)^2}\tau + \frac{\varphi_b^{1/2}}{(1-\varphi_b)^{5/2}} \int_0^{\tau} \left. \frac{\partial \varphi}{\partial \zeta} \right|_{\zeta_b} d\tau'. \tag{A8}$$

Appendix B: Dependence of Drainage on the Mean Bubble Radius Defined by the Fourth Moment r_{40}

The average velocity in a plateau border in terms of the liquid fraction is given by Eq. 7.

Substituting $V = (4/3)\pi r^3$ and $l = er$ into Eq. 7 and rewriting v in terms of r gives

$$v = \frac{c_v}{20\sqrt{3}\,\mu n_p} \frac{4\pi r^3}{3er} \frac{\varphi}{1-\varphi}(\rho g - A), \tag{B1}$$

where

$$A = \frac{\gamma}{2}\left(\frac{\delta n_p e r}{V} \right)^{1/2} (1-\varphi)^{-1/2} \varphi^{-3/2} \frac{\partial \varphi}{\partial z}. \tag{B2}$$

The capillary suction term in Eq. B1 represented by the term A is significantly smaller than the gravitational term during the simulation, except in the final stages of the simulation close to equilibrium. Therefore, the capillary suction term A can be discarded and the average velocity in a plateau border can be approximated by

$$v = \frac{\rho g \pi c_v}{15\sqrt{3}\,\mu n_p e}\left(\frac{\varphi}{1-\varphi} \right) r^2. \tag{B3}$$

The average flow rate Q in a plateau border is given by

$$Q = v a_p, \tag{B4}$$

where $a_p = \delta r_c^2$. Using Eq. 4, the cross-sectional area of a plateau border can be expressed in the form

$$a_p = \frac{4\pi}{3 n_p e}\left(\frac{\varphi}{1-\varphi} \right) r^2. \tag{B5}$$

Combining Eqs. B3, B4, and B5 gives

$$Q = B r^4, \tag{B6}$$

where

$$B = \frac{4\rho g c_v \pi^2}{45\sqrt{3}\, n_p^2 \mu e^2}\left(\frac{\varphi}{1-\varphi} \right)^2. \tag{B7}$$

The average flow rate through plateau borders for a range of bubble sizes can be expressed as

$$\langle Q \rangle = \int_0^\infty Q(r)F(r)\,dr, \tag{B8}$$

where $F(r)$ is the bubble-size frequency-distribution function in the foam column. Equation B8 can be expressed as

$$\langle Q \rangle = B\int_0^\infty r^4 F(r)\,dr. \tag{B9}$$

The mean bubble radius defined by the fourth moment is given by

$$r_{40} = \left(\frac{\int_0^\infty r^4 F(r)\,dr}{\int_0^\infty F(r)\,dr} \right)^{1/4} = \left(\int_0^\infty r^4 F(r)\,dr \right)^{1/4}. \tag{B10}$$

Thus

$$\langle Q \rangle = B r_{40}^4. \tag{B11}$$

Equation B11 shows that the mean bubble radius defined by fourth moment r_{40} is the appropriate bubble size for use with the present drainage equation.

Manuscript received Feb. 8, 2000, and revision received June 12, 2000.